Received: 1 July 2021 | Revised: 22 July 2021 | Accepted: 3 September 2021

DOI: 10.1002/suco.202100447

ARTICLE

fib CEB-FIP WILEY

Experimental investigation of the shear strength of one-way reinforced concrete (RC) slabs subjected to concentrated loads and in-plane transverse axial tension

Pablo G. Fernández | **Antonio Marí** | **Eva Oller**

Department of Civil and Environmental Engineering, Universitat Politècnica de Catalunya, Barcelona, Spain

Correspondence
Pablo G. Fernández, Universitat Politècnica de Catalunya, Department of Civil and Environmental Engineering, Campus Nord Jordi Girona 1-3, C-1 201, 08034 Barcelona, Spain.
Email: pablo.gonzalo.fernandez@upc.edu

Funding information
Ministerio de Economía y Competitividad, Grant/Award Number: BIA-2015-64672-C4-1-R

Abstract

This paper presents the results of an experimental campaign carried out to investigate the effects of in-plane transverse tensile forces on the shear strength of linearly supported one-way reinforced concrete (RC) slabs without shear reinforcement subjected to concentrated loads. A total of 5 half scale slabs (1650 × 1650 × 120 mm), subjected simultaneously to different levels of in-plane tensile forces and a concentrated load were tested up to failure. The clear shear span to effective depth ratio a_v/d was equal to 3 in all tests, to minimize the effects of the direct transmission of the load to the closest support, the so called arching action. As observed, the shear strength barely decreases with increasing values of the tensile force applied, even for values of the external force that cracked the concrete cross-section of the slabs in the direction perpendicular to the span. These observations may indicate that the shear–flexural behavior in the spanning direction is not significantly affected by the membrane forces in the transverse direction.

KEYWORDS

concentrated load, experimental campaign, one-way slabs, reinforced concrete, shear, tension

1 | INTRODUCTION

Reinforced concrete slabs are structural components widely used in both bridges and buildings, due to their great versatility and ease of construction. These structural elements are mainly subjected to bending and shear, but in some cases in practice, in-plane tensile stresses may arise and act simultaneously with the out-of-plane design loads. For instance, this situation may arise in top slabs of box girder bridges subjected to hogging bending moments, decks of tied arch bridges, floor slabs under seismic loads, restrained shrinkage, or thermal effects. The effect of tension on the shear strength of reinforced concrete elements has not been exhaustively studied throughout the last decades, but it is gaining attention within the last years.

1.1 | Previous research works

First widely known studies on the effect of tension on the shear strength of RC elements were carried out in the

Discussion on this paper must be submitted within two months of the print publication. The discussion will then be published in print, along with the authors' closure, if any, approximately nine months after the print publication.

United States, after the partial collapse of a military warehouse in 1955, by the Portland Cement Association.[1] Experiments conducted in that investigation, in which rectangular cross-section beams without stirrups were subjected to tension in the spanning direction, showed up to a 50% shear strength reduction for an axial tensile stress of 1.4 MPa. However, tested specimens were not heavily reinforced, having a flexural reinforcement ratio of 0.42%. Due to such a small amount of longitudinal reinforcement, the postcracking capacity was very low and failure occurred soon after first cracks formed. In the next decade, similar experiments using rectangular and T-shaped beams were conducted at the University of Washington.[2,3] After a series of experiments in beams with and without stirrups, it was recommended that the shear carried by the concrete should be taken equal to zero if tensile stresses exceed $0.33\sqrt{f_c}$ (f_c in MPa). This recommendation was incorporated into the ACI-318 building code[4] released in 1971, in which the concrete contribution to the shear strength was reduced linearly to zero as tensile stresses on the member increase to 3.4 MPa.

At the same time, another investigation carried out at the Imperial College,[5] rectangular beams subjected to different levels of tensile stresses, with a longitudinal reinforcement ratio of 1.46%, showed a moderate reduction on the shear strength with increasing tension, with a 12% decrement for the maximum tensile stress of 2.6 MPa applied. These results started to highlight the importance of the amount of longitudinal reinforcement on the shear strength of RC elements subjected to axial tension. A greater amount of reinforcement leads to narrower cracks and deeper compression head for a particular tension level, which contribute to enhance the shear strength.

In the early 1980s, two experimental campaigns conducted at Cornell University[6,7] for the US Nuclear Regulatory Commission studied the effects of Biaxial tension on the punching-shear strength of RC slabs (Figure 1a). Both studies concluded that the punching-shear strength was only slightly related to the biaxial tension level, although more flexible behavior was observed for higher levels of tension. Once again, worst results were obtained for the slabs with lowest reinforcement ratios in both orthogonal directions. In the same period of time, Regan[8] presented the results of an experimental campaign on the punching-shear strength of one-way and two-way slabs subjected to unidirectional in-plane tensile forces (Figure 1b). In both cases, an average 15% decrement of the ultimate load for an in-plane tensile stress of 3.95 MPa was reported.

In the late 1980s, as part of the validation of the Modified Compression Field Theory,[9] an experimental campaign was carried out at the University of Toronto,[10] where 24 square panels of 890 mm sides and 70 mm thickness, were subjected to different combinations of in-plane shear (v) and tension (σ_t). Panels were reinforced only in the longitudinal direction with a reinforcement ratio ρ of 1% or 2%, depending on the element. It was experimentally observed, as the MCFT had predicted, that panels have considerable postcracking shear capacity provided and that the longitudinal reinforcement ratio prevents excessive widening of the cracks. Panels with $\rho = 1\%$ showed almost no influence of tension on the shear strength up to values of σ_t close to 2 MPa, decreasing from that point onwards, until reaching the uniaxial tensile strength of 4.5 MPa. Panels with $\rho = 2\%$ showed an average 20% decrement of the shear strength when $\sigma_t \approx 4.5$ MPa and a 37% when $\sigma_t \approx 7$ MPa, highlighting once again the importance of the amount and distribution (the more uniform along the cross-section depth, the better) of longitudinal reinforcement. Similar trends were observed in another two experimental campaigns carried out several years after at the same laboratory in beam-like panels and square panels, respectively.[11,12]

More recently, laboratory tests were conducted at the Technical University of Denmark[13] in beams reinforced symmetrically using high performance steel ($f_y = 1027$ MPa) with a longitudinal tensile reinforcement ratio $\rho = 0.88\%$. Tested beams showed almost no influence of tension on the shear strength for tensile stresses up to 7.5 MPa. For this

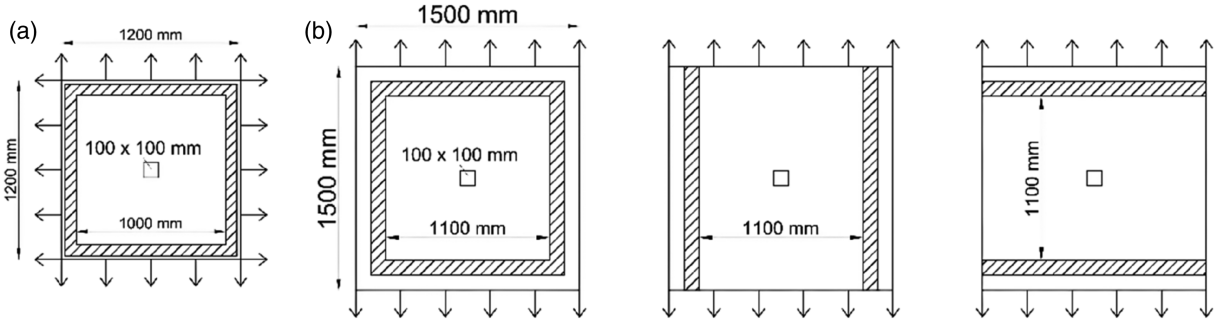

FIGURE 1 Set-up of the test carried out: (a) at Cornell University[6,7]; (b) by Regan[8]

level of tensile stress, for instance, Eurocode-2[14] predicts a total loss of shear strength. The use of high-performance concrete ($f_c > 75$ MPa) has also been studied.[15] In this case, T-shaped beams were tested under the simultaneous action of shear and axial tension, showing a 33% decrement for longitudinal tensile stresses for $\sigma_t = 1.81$ MPa when $\rho = 1\%$ and a 35% of reduction for $\sigma_t = 2.71$ MPa when $\rho = 1.51\%$. In both cases the reinforcement was concentrated close to the tension face.

First shear tests carried out in slabs subjected to uniaxial in-plane tension took place at the University of Lyon less than a decade ago.[16] Slabs were simply supported on their four sides and subjected to a point load close to one of the supports. The external in-plane tension was applied perpendicular to that support (Figure 2). All the tested slabs, reinforced non-symmetrically with a tensile longitudinal reinforcement ratio of $\rho = 1.22\%$, showed almost no influence of the longitudinal tensile stress for σ_t up to 0.65 MPa. However, a significant average reduction of a 27% was observed for $\sigma_t = 1$ and 1.2 MPa. These reduction percentages are more or less in line with the tests conducted on non-symmetrically reinforced T-shaped beams mentioned previously. Table 1 presents a summary overview of all these experimental work.

To conclude, within the last few years, thanks to all the research carried out, a couple of theoretical models to predict the punching-shear strength of two-way slabs subjected to in-plane uniaxial or biaxial tension have been presented.[17,18] Both models coincide in the importance of the amount of reinforcement parallel to the external tension. If the tensile stresses are high enough to cause concrete cracking, low reinforcement ratios may lead to a big loss of the punching-shear capacity caused by premature yielding of part of the reinforcement. However, more research is needed for the case of the shear strength of one-way slabs subjected to in-plane tension.

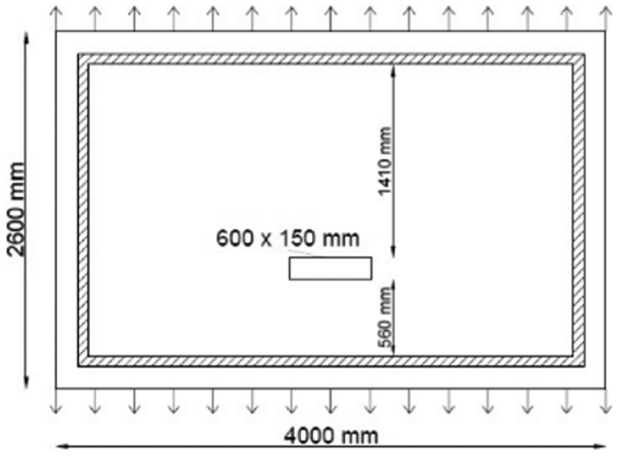

FIGURE 2 Set-up of the test carried out at the University of Lyon[16]

1.2 | Design codes

Shear provisions included in two of the most internationally accepted codes, such as Eurocode-2[14] and ACI 318-19[19] are reviewed in this section. EC-2, in section 6.2.2, indicates that the design value for the shear resistance $V_{Rd,c}$ is given by Equation (1), with a minimum value given by Equation (2), where γ_c is the safety factor for concrete; $k = 1 + \sqrt{200/d} \leq 2$ is the size effect factor; ρ_l is the amount of longitudinal tensile reinforcement ($\rho_l \leq 0.02$); b_w is the smallest width of the cross-section in the tensile area (mm); f_{ck} is the characteristic concrete compressive strength (MPa) and d is the effective depth of the cross-section (mm).

$$V_{Rd,c} = \left(\frac{0.18}{\gamma_c} \cdot k \cdot \sqrt[3]{100 \cdot \rho_l \cdot f_{ck}} + k_1 \cdot \sigma_{cp}\right) \cdot b_w \cdot d \quad (1)$$

$$V_{Rd,c} = \left(0.035 k^{3/2} \cdot f_{ck}^{1/2}\right) \cdot b_w \cdot d \quad (2)$$

The effect of axial stresses on the shear strength is included through the term $k_1 \cdot \sigma_{cp}$, where $k_1 = 0.15$ and $\sigma_{cp} = N_{Ed}/A_c$, being N_{Ed} the axial load applied in the cross-section, with negative sign in the case of tension, and A_c is the area of the concrete cross-section. It is remarkable that EC-2 considers that the increment of shear strength due to a compression force C is equal to the reduction in shear strength due to a tensile force of the same magnitude, despite the response of concrete in one case or in the other one is radically different. Another important aspect of this formulation is that it is intended mostly for beams, where axial stresses are always applied in longitudinal (spanning) direction. However, if these expressions are used to calculate the shear strength of a one-way slab, axial loads may exist in the longitudinal and in the transverse direction. If the latter is the case, it is not clear whether those axial stresses have to be taken into account or neglected. The experimental campaign presented in this paper tries to provide some insight into this issue.

ACI 318-19 provides different sets of equations to calculate the shear strength, depending on the type of element and loading. Chapter 7: "*One way slabs*" refers to section 22.5 for the calculation of the concrete contribution to the shear strength V_c. Within this section, it is pointed out that the effect of axial tension due to creep and shrinkage shall be considered in calculating V_c, and it is recommended that if there is uncertainty about the magnitude of the axial tension, it is desirable to design shear reinforcement to resist the total shear. For elements without shear reinforcement, and assuming normal weight concrete ($\lambda = 1$), Table 22.5.5.1 of ACI Code

TABLE 1 Experimental work overview

Author	Element type	ρ (%)—symmetric	Findings on shear strength
1	Beam	0.45—NO	50% reduction for $\sigma_t = 1.4$ MPa
2, 3	Beam	(1–3)—NO	$V_c = 0$ if $\sigma_t = 0.33\sqrt{f_c}$ (MPa)
5	Beam	1.46—NO	12% reduction for $\sigma_t = 2.6$ MPa
6, 7	Slab	(1–3)—YES	Punching-shear strength only slightly affected
8	Slab	1.3—YES	15% reduction for $\sigma_t = 3.95$ MPa
10, 11, 12	Panel	(1, 2)—YES	No influence for $\sigma_t < 2$ MPa if $\rho = 1$ 20% reduction for $\sigma_t = 4.5$ MPa if $\rho = 2$
13	Beam	2—YES	$f_y = 1027$ MPa. No influence for $\sigma_t < 7.5$ MPa
15	Beam	(1–1.5)—NO	$f_c > 75$ MPa. 33% reduction for $\sigma_t = 1.81$ MPa if $\rho = 1$ $f_c > 75$ MPa. 35% reduction for $\sigma_t = 2.71$ MPa if $\rho = 1.5$
16	Slab	1.22—NO	30% reduction for $\sigma_t = 1.2$ MPa

provides Equation (3) for the one-way shear strength of non-prestressed members, where $\lambda_s = \sqrt{\frac{2}{1+0.004d}} \leq 1$ is the size effect factor; ρ_w is the amount of longitudinal tensile reinforcement; f'_c is the specified concrete compressive strength (MPa); b_w is the web width (mm); and d is the distance from the extreme compression fiber to centroid of longitudinal reinforcement (mm).

$$V_c = \left[0.66 \cdot \lambda_s \cdot (\rho_w)^{1/3} \cdot \sqrt{f'_c} + \frac{N_u}{6A_g}\right] \cdot b_w \cdot d \qquad (3)$$

In this case, the effect of axial stresses is included trough the term $N_u/6A_g$, where N_u is the axial force normal to the cross-section acting simultaneously with the shear force ($N_u < 0$ for tension) and A_g is the gross area of concrete. In the same way as EC-2, ACI-318 considers the increment of shear strength due to a compression force equal to the reduction in shear strength due to a tensile force of the same magnitude. According to the definition of N_u, it seems that it is intended for axial forces parallel to the spanning direction, and it is not clear what to do in the case of a one-way slabs subjected to axial tension in the transverse direction.

In this context, an experimental campaign has been carried out at the Laboratory of Technology of Structures and Materials of the Universitat Politècnica de Catalunya (UPC), whose main goal was to identify and quantify the effect of unidirectional in-plane tension forces perpendicular to the spanning direction on the one-way shear strength of RC slabs.

2 | EXPERIMENTAL CAMPAIGN

2.1 | Specimens tested

A total of five 1650 × 1650 × 120 mm slabs, simply supported on two parallel linear supports, were cast at the Laboratory of Technology of Structures and Materials of the Universitat Politècnica de Catalunya (UPC). The dimensions of the slabs tested in the context of this experimental campaign were conditioned by punching-shear tests previously performed by the authors,[20] with the aim of reusing the tensioning system built for that occasion. In order to ease the placement, alignment and removal of the whole set-up within the portal frame where the main hydraulic jack of the laboratory is installed, the point load was decided to be applied at the center of the slabs. This way, one of the supports was moved inwards so a clear shear span to effective depth ratio a_v/d equal to 3 was attained. The opposite support was also moved slightly inwards in order to avoid a flexural failure. The final dimensions of the set-up are and the supporting system are shown in Figure 3.

The specimens were subjected to tension in their plane, only in the direction parallel to the supports, through 10 posttensioning bars 25 mm in diameter and 600 mm in length (Figure 4), partially embedded in two opposite faces (5 bars on each side) connected to the tensioning system. Although most of the tension was transmitted to the concrete by bond, anchors were placed at the embedded end of the bars for greater safety. The value of the external tension applied during the tests is measured in relation to the tensile force producing the cracking of the slab's cross-section, or $T_{cr} = A_c \cdot f_{ct}$, with A_c being the composite concrete and steel area of the cross-section of the slab and f_{ct} the concrete tensile strength. Averaging the values of the tensile strength obtained from characterization tests (Table 2), $T/T_{cr} = 1$ approximately correspond to $\sigma_t = 3.2$ MPa.

The slabs were reinforced with two steel meshes arranged on the upper and lower faces (Figure 5). In the direction parallel to the external tension (transverse direction), all the tested slabs, named A4, A5, A6, A7, and B2, were symmetrically reinforced. On each face,

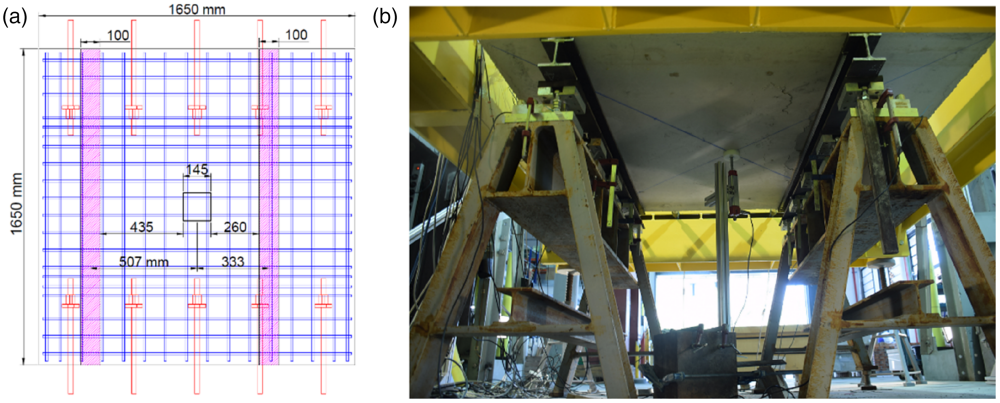

FIGURE 3 Experimental set-up: (a) dimensions of the specimens; (b) bottom view of a tested specimen

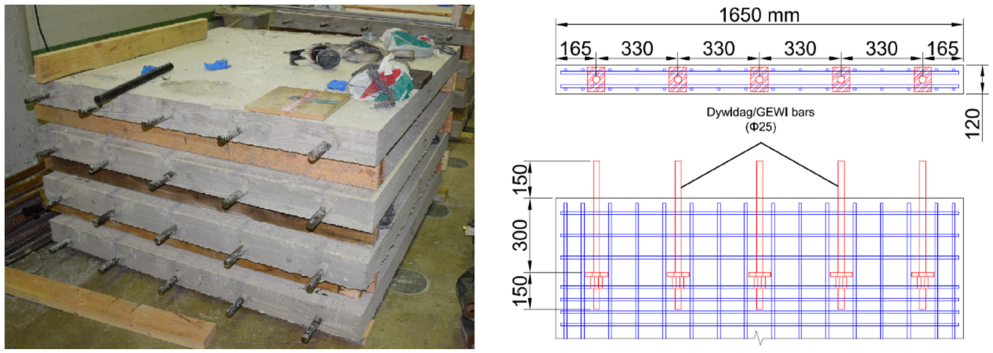

FIGURE 4 Position of posttensioning bars inside the slabs

TABLE 2 Mean values of material properties

Concrete					
Slab	f_c **(MPa)**	f_{ct} **(MPa)**	E_c **(GPa)**	a_g **(mm)**	**Age (days)**
A4	36.2	3.01	28.5	10	170
B2	36.6	3.23	31.3	10	287
A5	37.5	3.27	29.8	10	277
A6	37.0	3.40	29.6	10	280
A7	35.9	3.12	30.0	10	184
Steel					
Diameter (mm)			f_y **(MPa)**		E_s **(GPa)**
10			526		216.3
12			535		210.7
16			535		201.6

reinforcement consisted of 12 mm bars spaced 105 mm in type A slabs ($\rho = 0.011$) and 16 mm bars spaced 105 mm in slab B2 ($\rho = 0.02$).

In the direction perpendicular to the applied tension (longitudinal or spanning direction), on the lower face, an assembly consisting of 12 mm bars spaced 100 mm was arranged in all cases, ($\rho = 0.013$), while 12 mm bars spaced 200 mm were arranged on the upper face. Additional reinforcing bars were placed in the vicinity of the posttensioning bar anchors, as a measure of local reinforcement. The tensile reinforcement ratio and effective depth of each type of slab are shown in Table 3. The amount of transverse reinforcement in specimen B2 ($\rho = 2\%$) is higher than usual in practical cases. However, the experimental results of this specimen can be adequate to identify if the increment of the reinforcement parallel to tension significantly affects the structural response and the shear strength.

The slabs were cast using ready-mixed concrete from a local supplier. Normal strength concrete C30/37 with

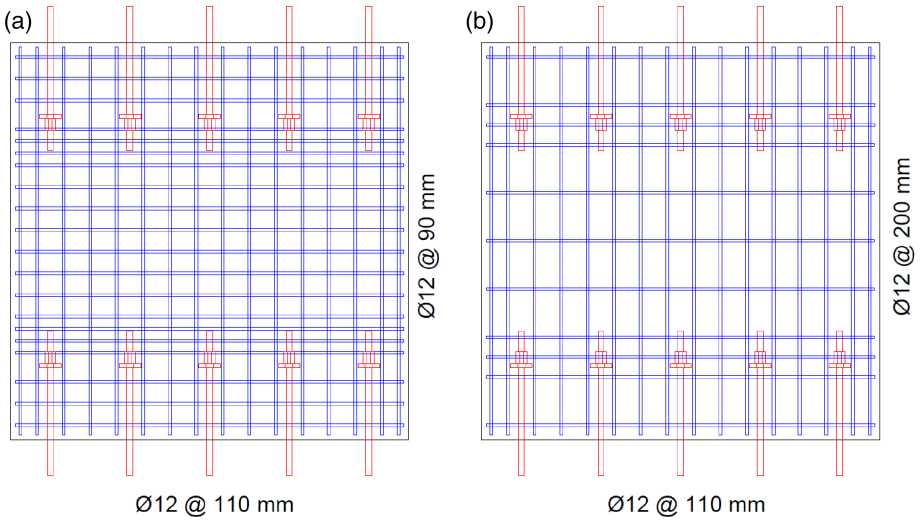

FIGURE 5 Reinforcement layout for type-A slabs: (a) bottom face; (b) top face

TABLE 3 Reinforcement ratios and effective depth of the tension face reinforcement

	Parallel to tension			Perpendicular to tension		
Slab type	Reinforcement area (mm^2)	Reinforcement ratio	Effective depth (mm)	Reinforcement area (mm^2)	Reinforcement ratio	Effective depth (mm)
A	1810	0.0108	99	1810	0.0130	87
B	3217	0.0197	97	1810	0.0133	85

crushed limestone aggregate with a maximum size of 10 mm was used. To characterize the concrete, standard compression (UNE-EN 12390-3), splitting (UNE-EN 12390-6), and elastic modulus (UNE-EN 12390-13) tests were performed. The specimens were reinforced with deformed bars of B500-S steel. Yield stress and elastic modulus of each type of reinforcing steel (UNE-EN ISO 6892-1) were also characterized. Results are shown in Table 2.

2.2 | Test set-up

Four out of the five tested specimens were subjected to different levels of in-plane tension, while the control slab was tested without axial force. To introduce the tensile force in the slabs, an auxiliary steel structure, whose plan dimensions were 2500 × 2840 mm, was used. This structure consisted of a rectangular steel frame surrounding the slab (Figure 6a). On sides parallel to the tensile forces, the frame consisted of a single HEB 300 profile, whereas on both perpendicular faces it was formed by two HEB 300 profiles arranged in parallel and slightly separated to allow the passage of bars (extensions) connected to the aforementioned bars partially embedded in the slab (Figure 6b). On one of these faces, a passive anchorage for the tensioning bars was used while they were prestressed from the other end, with the help of force-controlled hollow jacks connected to the bars protruding from the specimens (Figure 6c).

The steel structure was set at the appropriate height with the help of four height-adjustable supports located under each of the four corners of the frame. For safety reasons, once the desired external force value was reached, the bars were anchored and the jacks were disconnected from them. This fact caused a small loss of the axial force during the test that was quantified by the arranged instrumentation. The theoretical loads to be applied and the values measured during the tests are shown in Table 4.

Supporting system comprises two HEB 100 profiles 1650 mm long placed on top of five 20 × 120 mm hinged load cells used to measure the distribution of the reaction at each support (Figure 7). A piece of rubber 120 × 120 × 20 mm was placed over each of the load cells to allow the free rotation of the slab. A 10-mm thick rubber strip was placed on top of the HEB 100 profiles to ensure smooth contact between the supports and the tested specimens. Load cells were supported on two rigid easels arranged in such a way that the distance between the inner face of the loading plate and the closest support was equal to $3d$ ($a_v = 3d$).

To introduce the concentrated load, a hydraulic jack anchored in a loading frame, rigidly fixed to the floor

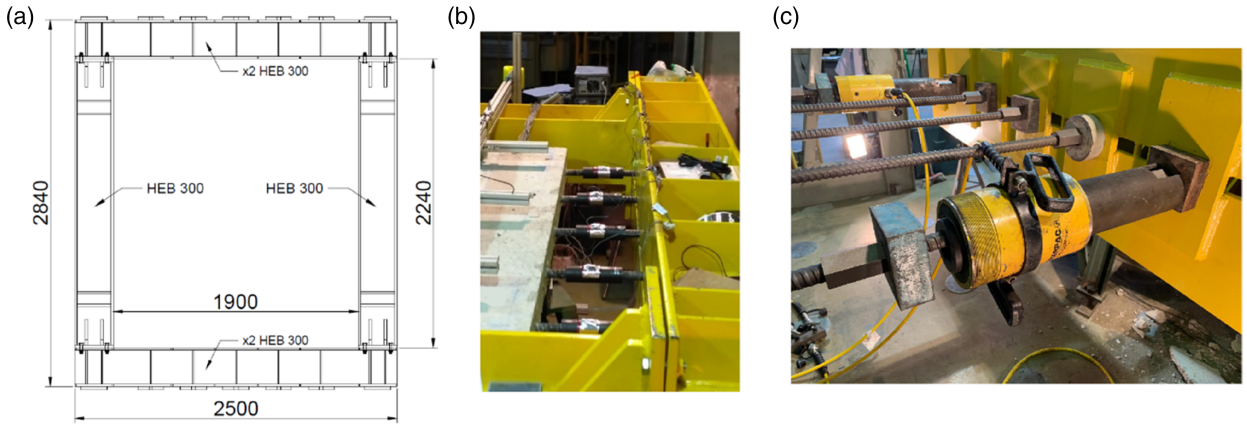

FIGURE 6 Tensioning system used to apply the axial force to the specimens: (a) steel frame; (b) extension connected to the protruding bars; (c) jacks placed at the active anchorage

TABLE 4 Values of the tensile force applied at each test

Slab	T/T_{cr} before disconnecting jacks	T/T_{cr} at the test beginning	T/T_{cr} at failure
A4	0.00	0.00	0.00
B2	0.50	0.45	0.43
A5	0.80	0.73	0.70
A6	1.10	1.08	1.06
A7	1.40	1.32	1.30

FIGURE 7 Support system for the tested specimens

slab, with a maximum capacity of 1000 kN was used. The out-of-plane load was applied to the specimens through a 145 × 145 × 30 mm steel plate, under which a thin layer of fine aggregate was placed to ensure regular contact with the upper face of the slabs.

2.3 | Instrumentation

In addition to the load cells of 50 kN placed underneath the supports, hollow load cells of 500 kN were used in the posttensioned bars (Figure 8a), in both active and passive anchorages, in order to measure the in-plane tensile force applied to each slab. To control the possible yielding of the reinforcement, in both longitudinal and transverse direction, 8 strain gauges were distributed as shown in Figure 8b. To measure the deflection underneath the point load of each specimen, a 75 mm displacement transducer was positioned at the center of the lower face, jointly with the internal linear variable displacement transducer (LVDT) of the loading frame. Finally, 3 LVDTs were placed in the vertical of each support on the upper side of the slabs, to control their descent and then, to subtract their mean value from the displacements measured in the center of the slab.

2.4 | Test procedure

First, the tensile force, given in Table 4, was introduced in the slabs and, subsequently, the point load was incrementally applied on its center up to failure of the specimen. In all cases, two levels of the out-of-plane load were previously applied and removed, one up to 40 kN and another up to 80 kN. Both loads were maintained for 100 s and served to accommodate all the elements

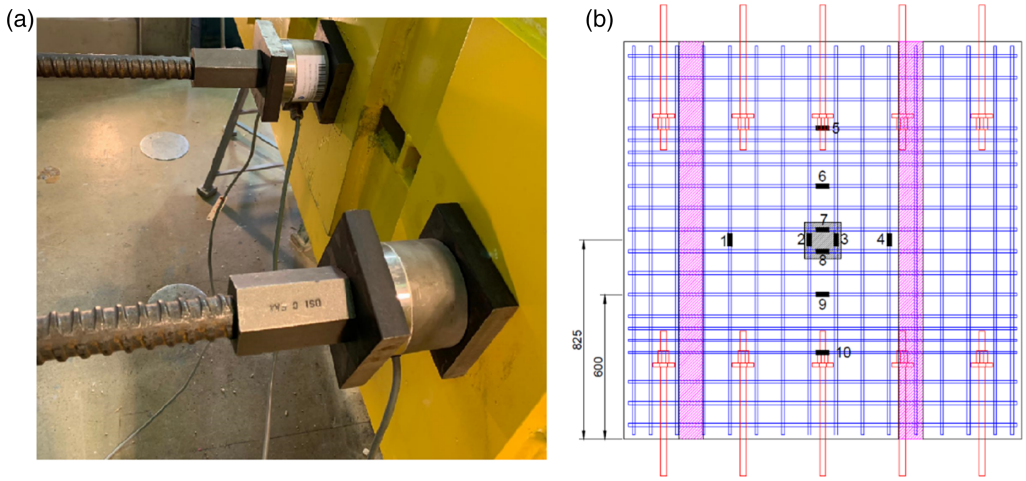

FIGURE 8 (a) Hollow load cells placed at the anchorages of the tensioning bars; (b) position of the strain gauges

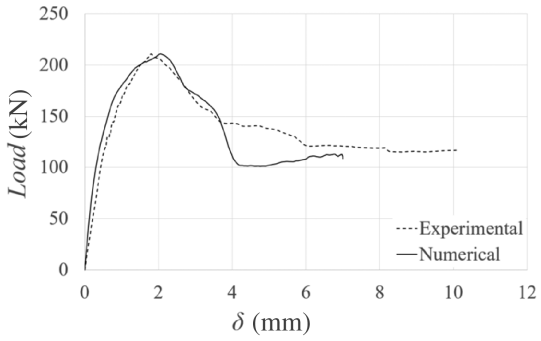

FIGURE 9 Load–deflection curve of the type-A control slab (A4) obtained in the lab test and with FEM

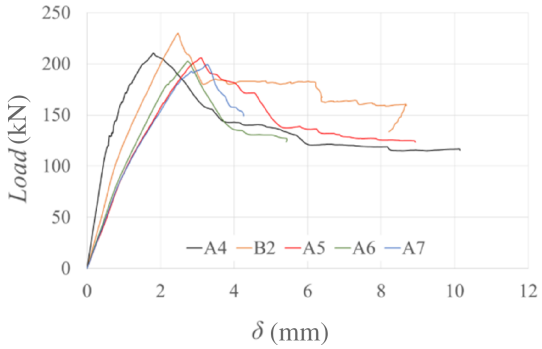

FIGURE 10 Load–deflection curves of the experimental tests

involved in the test and to check that the instrumentation was properly working. Once the second test load ended and the slab was unloaded, the test up to failure was started, applying the load by a controlled displacement at a rate of 0.005 mm/s.

In support of the experimental campaign, a finite element model using software package Simulia Abaqus was developed, taking as reference previous works carried out by the authors[20] and Nana et al.[21] This model was initially used to predict the tests results and to design the auxiliary structures of loading and support. Once the test on the control slab was performed, the numerical model was calibrated with the obtained result (Figure 9) and used to predict the shear strength of the rest of Type-A slabs under the corresponding value of the external force applied. With respect to Type-B slab, only a single test was performed with a tensile force of $T/T_{cr} = 0.43$. Then, since there was not reference slab of type B, the same numerical model was also used to predict the shear capacity of the Type B reference slab, as shown in Table 5. Details of the numerical simulations will be explained in Section 4.

3 | EXPERIMENTAL RESULTS

3.1 | Ultimate loads

The main interest of the experimental campaign was to quantify the variation of the shear strength as a function of the tensile force applied to the slabs. Figure 10 shows

TABLE 5 Punching strength values of both types of control slabs

Type of slab	Ultimate load (P_u) (kN)	Shear strength ($V_{u\ control}$) (kN)	Type of analysis
A	210.6	127.1	Lab. Test
B	230.2	138.1	FEM

TABLE 6 Test results

Slab	$V_{u,\text{control}}$ (kN)	T/T_{cr} at failure	Ultimate load (P_u) (kN)	Shear strength (V_u) (kN)	$V_u/V_{u,\text{control}}$
A4	210.6	0.00	210.6	127.1	1
B2	230.2[a]	0.43	225.3	135.9	0.979
A5	210.6	0.70	206.9	124.4	0.978
A6	210.6	1.06	202.8	122.4	0.963
A7	210.6	1.30	199.4	119.6	0.947

[a]Obtained from FEM.

the comparison between all the experimental load–deflection curves obtained. As can be seen, the ultimate load of all type-A slabs slowly decreases with increasing levels of the applied tensile force, with a 5.3% reduction for $T/T_{cr} = 1.3$ ($\sigma_t = 4.2$ MPa). The whole trend is showed in Figure 16. Regarding slab B2, the ultimate load obtained was a 2.1% lower than that obtained for its control slab using the aforementioned FEM, confirming the trend observed with type-A slabs. Values of the ultimate load and comparison to the control slabs are summarized in Table 6. These results indicate that, for the tension level applied in the laboratory tests, if this tensile force is applied in the direction perpendicular to the span, the shear strength seems to be barely affected.

Nevertheless, the external tension affected the stiffness of the specimens. Slabs A5, A6, and A7 showed similar response, which indicate that the external force cracked the concrete, but the reinforcement was able to carry all the stresses caused by the addition of transverse bending and tension. This was confirmed by the measurements provided by the strain gauges placed in both longitudinal (gauges 7 and 8) and transverse (gauges 2 and 3) reinforcement underneath the point load. No signs of yielding were observed in any of the experimental tests, which discards the possibility of a flexural failure. These measurements are in good agreement with the brittle failure observed in the load–deflection curves. Slab B2 represents an intermediate situation, in which concrete cracks prematurely, but the higher reinforcement ratio in the transverse direction increases the global stiffness with respect to type-A slabs. It is interesting to note that slab B2 presented a higher shear strength than slab A4 (type-A control slab). Some numerical studies[22] have shown a small but positive influence of the transverse reinforcement ratio on the shear strength. However, no significant influence has been observed experimentally.[23–25] In the context of the study presented herein, the FEM predicted a 9.3% increment of the shear strength for the type-B control slab with respect to the A4 control slab, and slab B2, tested with a tension level of $T/T_{cr} = 0.43$ ($\sigma_t = 1.38$ MPa), resisted a shear strength value 7.1% higher than the control slab A4.

Figure 11 shows the state of cracking at the bottom face of the slab at failure for all the tests carried out. Auxiliary lines at 45° with the spanning direction have been superimposed as a reference. As can be observed, a crack parallel to the closest support appeared in all cases. In slabs subjected to tension, this failure crack was observed to turn and to connect with cracks parallel to the spanning direction provoked by the external force applied. Only slab A6 presented a cracking pattern that seems to be a transition between shear and punching-shear failure, since the crack parallel to the support quickly turns and partially surrounds the loading plate. Negative influence of in-plane tensile forces on the punching-shear strength of two-way slabs have been reported,[17,18] and this may have been the case of slab A6. However, as shown in Figure 10 and Table 6, the load-deflection behavior and the ultimate load of this slab were in accordance with the rest of results obtained.

3.2 | Reactions at the supports

In order to know if the external tensile force affected the distribution of the reactions at the supports, the measures yielded by the load cells supporting both HEB 100 profiles were analyzed and compared with the values obtained for the control slab. Despite only five load cells were available for each support, it was enough to capture the global behavior. Figure 12 shows the distribution of the reaction at both supports for all type-A slabs tested. It can be seen that regardless the level of tensile force applied, reaction distributes more or less in the same way, with highest values measured at the center of each support and decreasing toward the free edges of the slab. An interesting point is that, despite the clear shear span for the farthest support is equal to $5d$, it was observed a similar trend for the reaction distribution than that at the support placed at $3d$. This observation is in agreement with some existing studies[26,27] which conclude that a limit value for the horizontal load spreading must be established in order to avoid highly un-conservative results when using the simplified formulation of the codes.

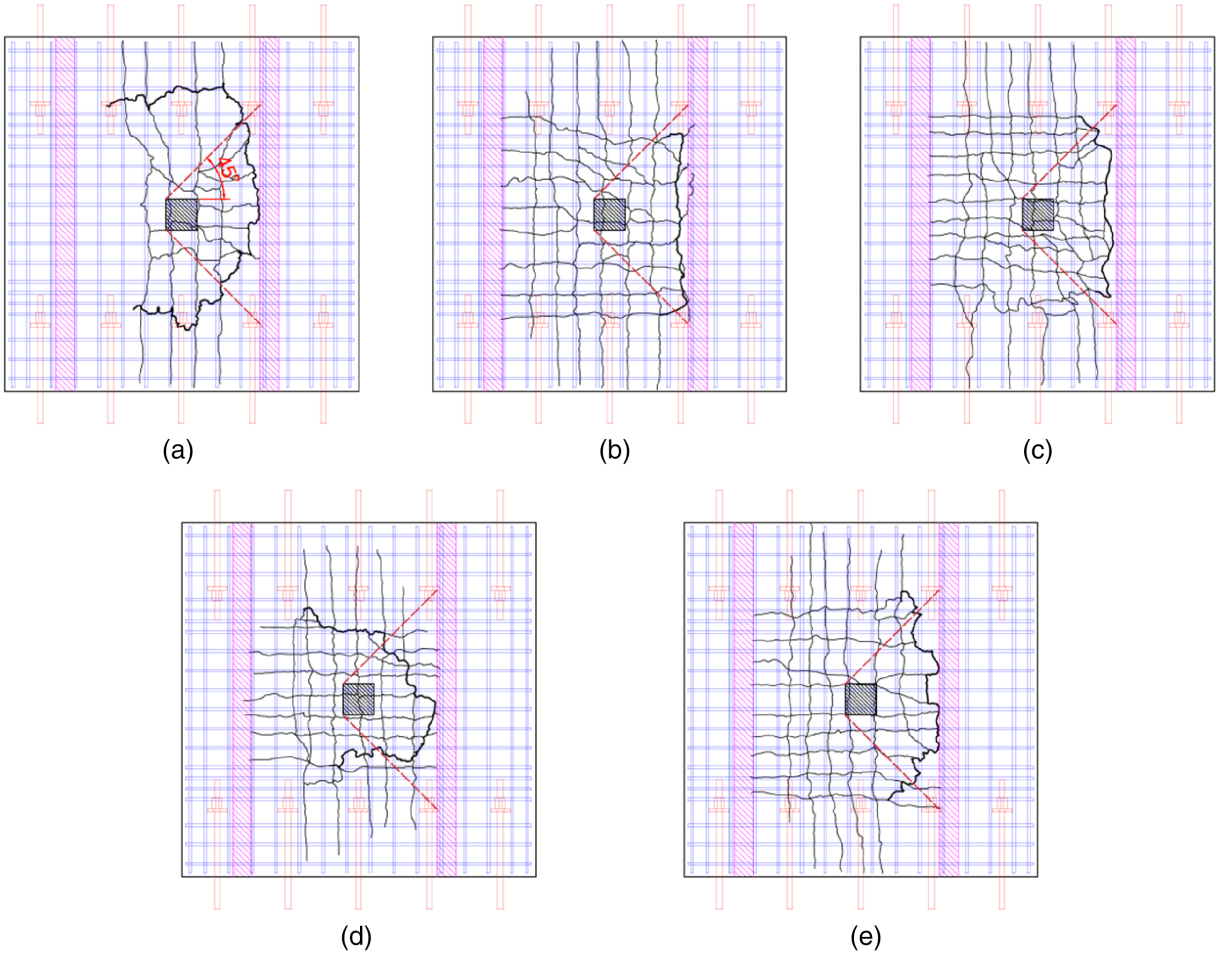

FIGURE 11 Cracking patterns at failure. (a) A4 ($T/T_{cr} = 0$); (b) B2 ($T/T_{cr} = 0.43$); (c) A5 ($T/T_{cr} = 0.7$); (d) A6 ($T/T_{cr} = 1.06$); (e) A7 ($T/T_{cr} = 1.3$)

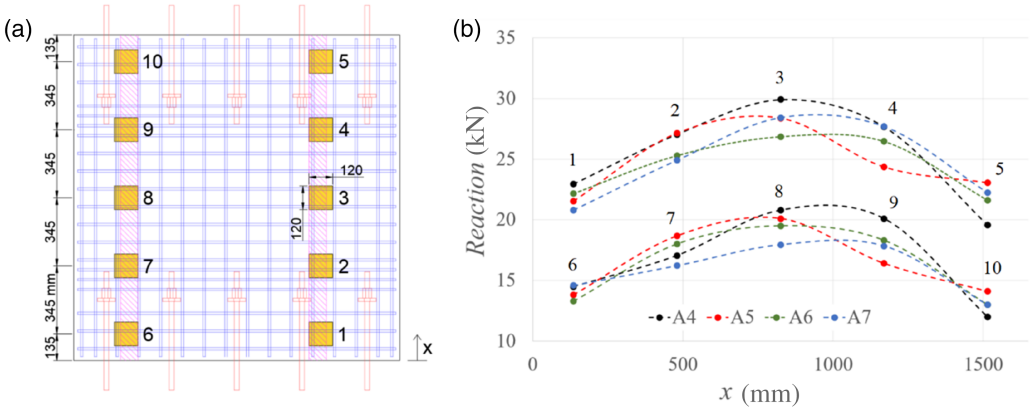

FIGURE 12 (a) Position and dimensions of the load cells placed underneath the support; (b) distribution of the reaction at failure at the closest support to the point load for type-A slabs

4 | NUMERICAL SIMULATIONS

This section presents the numerical model developed jointly with the experimental campaign. In addition to help in the design of the test set-up, the model was also used to contrast the values of the shear strength obtained experimentally, and to perform simulations for values of the tensile force different from those applied in the experimental campaign. The numerical model was carried out with the help of Simulia Abaqus software.[28]

4.1 | Model generation

Taking into account the existing plane of symmetry at the middle of the slab, parallel to the spanning direction, both in geometry and loading, only half of each slab was modeled, considering the corresponding boundary conditions in the symmetry plane. The numerical model was inspired in a similar model developed by the authors to study the influence of in-plane tensile forces on the punching-shear strength of RC slabs,[20] but also recommendations given in Nana et al.,[21] as the use of an explicit quasi-static solution or a linear evolution of the damage parameter, in both tension and compression.

Regarding the type of element used, 8 nodes hexahedral elements with reduced integration (C3D8R) were selected for concrete in order to reduce the computational cost and to avoid obtaining excessively rigid results due to the linear interpolation of the displacements field. For the reinforcing bars, linear beam elements of 2 nodes (B31) perfectly bonded to concrete were used. The chosen size for the concrete elements was 20 mm, so that six elements were arranged along the 120 mm of the slab thickness. The same element size of 20 mm was considered for the reinforcing elements. The supports of the slab were simulated by means of non-linear springs (SPRING A), with a very high stiffness in compression and practically zero stiffness in tension, thus allowing the partial lifting of the slab and avoiding the appearance of undesired tensile reactions (Figure 13a). The introduction of tensile forces was simulated in the model by applying the loads directly to the nodes located in the area of the anchor plates of the posttensioning bars (Figure 13b), while for the point load, a displacement was imposed on the nodes located on the upper face of the slab, under the surface occupied by the load plate (Figure 13c).

The simulations were performed by means of a quasi-static analysis, available in the Abaqus/Explicit package. This kind of analysis has several advantages in comparison to the traditional implicit method when non-linear analyses are carried out. The absence of a global tangent matrix stiffness in the explicit analysis avoids certain convergence problems and in general, it saves a substantial amount of time when performing parametric studies. To avoid dynamic instabilities, the ratio of the kinetic energy generated by the inertia forces to the internal deformation energy must be negligible, which has to be checked after each simulation.

4.2 | Material modeling

To simulate the behavior of concrete, the Concrete Damaged Plasticity model was chosen,[29,30] which requires the definition of the uniaxial constitutive equations in compression and tension, in addition to the definition of a yielding surface and, optionally, damage parameters for the Young's modulus also in tension and compression. In compression, a linear behavior of up to 40% of f_c (σ_{c0}) was considered. To define the elastic response, only the modulus of elasticity E_c and the Poisson ratio ν are needed. The modulus of elasticity is that obtained in the corresponding characterization test (see Table 2), while for ν, as Abaqus considers it a fixed value throughout the whole simulation process, including the postcracking regime, a value $\nu = 0$ was chosen. To take into account the non-linear behavior in compression, the Hognestad parabolic constitutive equation was chosen (Figure 14a). The values of ε_{c0} and ε_{cu} correspond to those proposed in table 3.1 of EC-2, with values of $\varepsilon_{c0} = 0.0020$ and $\varepsilon_{cu} = 0.0035$. As mentioned above, a linear increment for

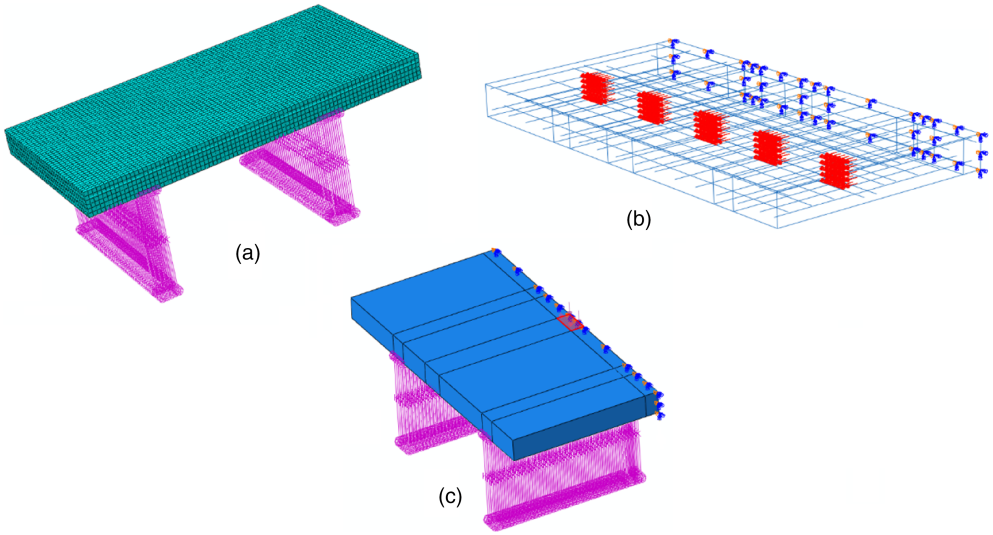

FIGURE 13 Modeling techniques: (a) mesh sizes and spring simulating the supports; (b) area of application of the tensile force; and (c) imposed displacement at the point load position

the damage parameter d_c was selected, with a maximum value of $d_c = 0.9$ corresponding to $\varepsilon_c = \varepsilon_{cu}$ to avoid convergence issues (Figure 14b).

Regarding the tensile behavior, the model proposed in section 5.1.8.2 of the Model Code 2010[31] has been used, which considers a linear behavior up to cracking stress f_{ct}, and a bilinear softening branch governed by the fracture energy of the material (Figure 14c). The value of the fracture energy adopted is given by Equation (4), proposed in Cladera et al.[32] as a modification of that provided by the Model Code 2010 to account for the maximum aggregate size of concrete, which in this case was 10 mm. A linear variation of the damage parameter in tension d_t was considered, similar to the one in compression, but this time depending on the crack width w rather than on the plastic strain ε_{pl}. A maximum value of $d_t = 0.9$ corresponding to $w = w_c$ was chosen also to avoid convergence issues (Figure 14d).

$$G_f = 0.028 f_c^{0.28} d_{d_{\max}}^{0.32} \tag{4}$$

The behavior of concrete in tension was introduced in ABAQUS through a stress–strain relationship, so it was necessary to transform the stress-crack width given by Model Code (Figure 14c) into a stress–strain curve. For this purpose, the crack opening is divided by the characteristic length of the element (l_c), defined as the average dimension of a finite element, in this case the length of an edge of a cubic element. Thus, the softening of the tensile branch, is given by $\varepsilon_{ct} = \varepsilon_{cr} + w/l_c$, where ε_{cr} is the concrete strain corresponding to the tensile strength, f_{ct}.

The values used to define the yielding surface were modified from those proposed in Fernandez et al.[20] to adjust the simulation of the type-A control slab to the results obtained in the laboratory (Figure 9), and are collected in Table 7. For the steel reinforcement, a bilinear stress–strain diagram was used, considering perfect plasticity. Yield stress and Young's modulus were extracted from the characterization tests (see Table 2).

4.3 | Results

A comparison between the load–displacement curves obtained by the numerical simulations and experimentally is shown in Figure 15. Accurate results were obtained in terms of ultimate load and deflection, despite numerically obtained shear strengths are in general smaller than the experimental ones, with an average difference of 4.46%. Results of the comparison are summarized in Table 8.

Once the numerical model was validated with the experimental results, simulations were performed, for type-A slabs, for other values of T/T_{cr} than those applied at the laboratory, up to a maximum of $T/T_{cr} = 1.5$ (Figure 16). A linear decreasing trend is observed, with a

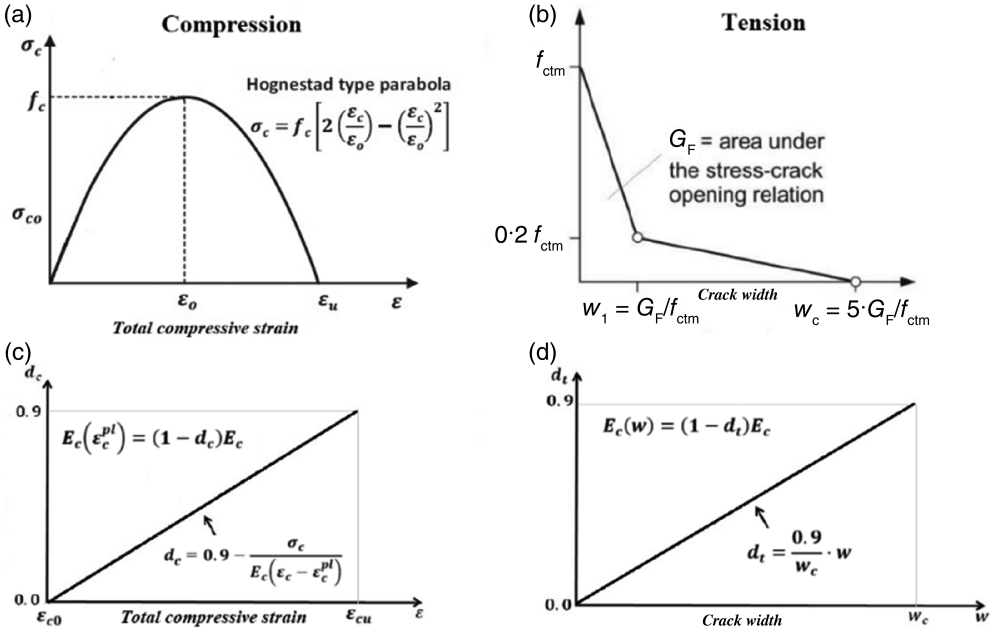

FIGURE 14 Constitutive relationships for concrete: (a) compressive behavior; (b) compressive damage; (c) tensile behavior; and (d) tensile damage

TABLE 7 Parameters defined for the concrete damaged plasticity

Dilation (ψ)	Eccentricity (ϵ)	σ_{b0}/σ_{co}	K	Viscosity (μ)
36.0	0.1	1.16	0.8	0

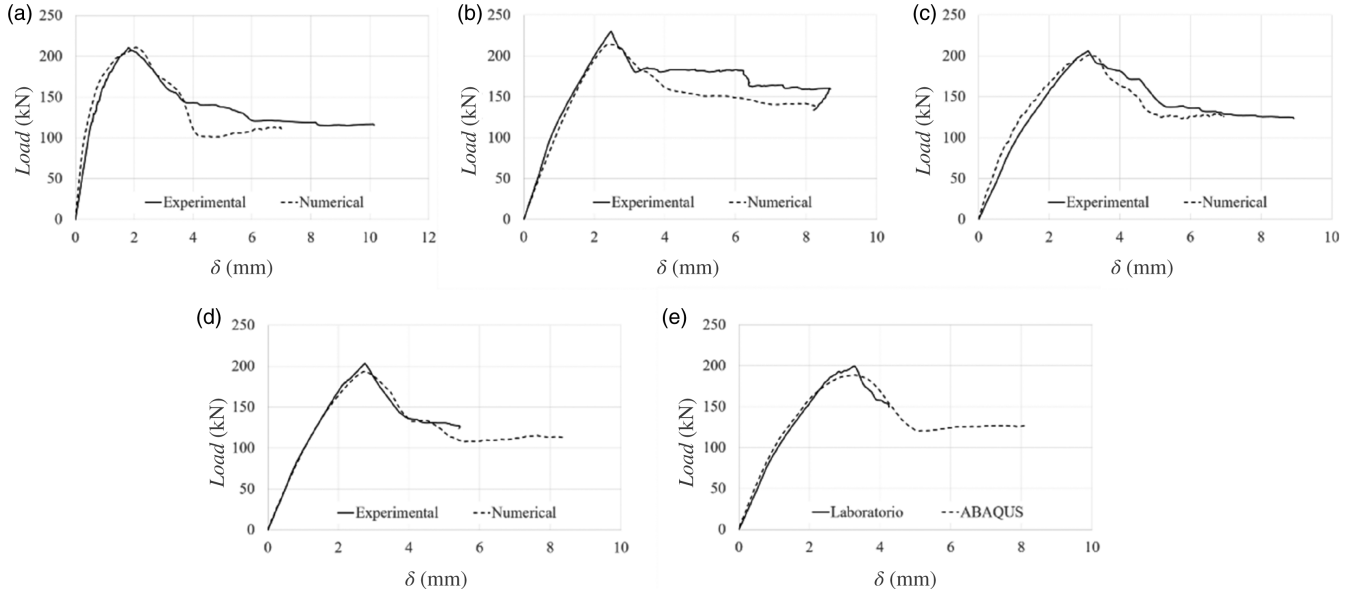

FIGURE 15 Comparison between load-deflection curves obtained with the numerical model and experimentally: (a) A4 ($T/T_{cr} = 0$); (b) B2 ($T/T_{cr} = 0.43$); (c) A5 ($T/T_{cr} = 0.7$); (d) A6 ($T/T_{cr} = 1.06$); and (e) A7 ($T/T_{cr} = 1.3$)

FIGURE 16 Comparison of the relative decrement of the shear strength obtained numerically, in laboratory tests and with EC-2 and ACI-318 predictions

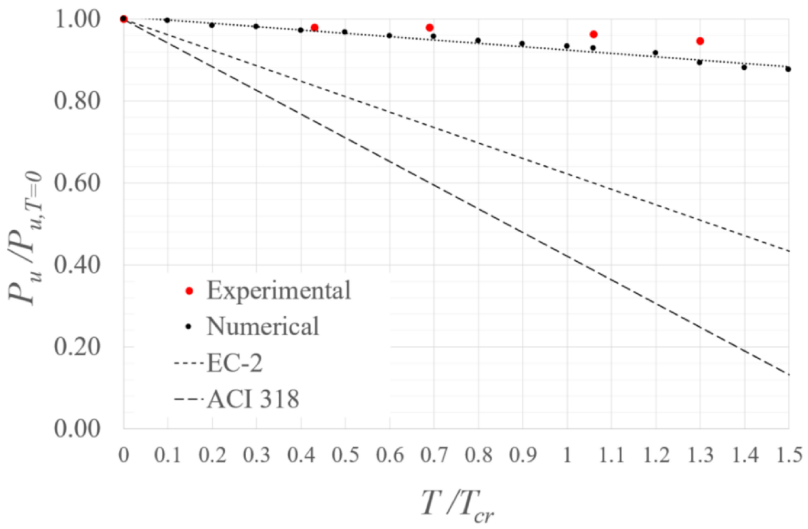

weak interaction between shear strength in the spanning direction and tensile stresses in transverse direction. For $T/T_{cr} = 1.2$ ($\sigma_t \approx 3.8$ MPa), $P_u/P_{u,T=0}$ ratio is equal to 0.92. Beyond that point, the numerical model predicts a slightly greater reduction of the shear strength as the tensile force increases, with a 12.4% decrement when $T/T_{cr} = 1.5$ ($\sigma_t \approx 4.8$ MPa). In general, numerical simulations are in agreement with the experimental results. As can be seen, B2 slab properly fits the curve obtained for type-A slabs, which may indicate that for the considered reinforcement ratios, the effect of the external tensile force on the shear strength is similar.

Figure 16 also includes EC-2 and ACI 318 predictions (Equations (1) and (3), respectively) for the reduction of the shear strength with increasing tension. For their calculation, the value of the transverse tensile stress has been used without any further consideration, assuming that longitudinal and transverse normal stresses affects the same way the shear strength. As can be seen, this approach leads to highly conservative results. For example, for $T/T_{cr} = 1.3$ ($\sigma_t \approx 4.2$ MPa), EC-2 predicts a 49.2% reduction and ACI 318 a 75.3% reduction. This percentages are much greater than the 5.3% reduction observed experimentally and 10.8% reduction predicted numerically for the same level of tension. Therefore, in order to obtain closer results to those obtained experimentally and numerically, the value of the transverse tensile stress should be weighted before being used in the current code formulations.

Nevertheless, since the effect of normal stresses is an additive term in the shear strength, this factor may change

TABLE 8 Comparison between numerical and experimental results

Test no.	T/T_{cr}	P_u (numerical) (kN)	P_u (experimental) (kN)	$P_u/P_{control}$ (numerical)	$P_u/P_{control}$ (exp.)
1	0	210.95	210.61	1	1
2	0.43	214.03	225.30	0.930	0.979
3	0.70	200.63	206.09	0.951	0.978
4	1.06	193.59	202.86	0.918	0.963
5	1.30	188.24	199.42	0.892	0.947

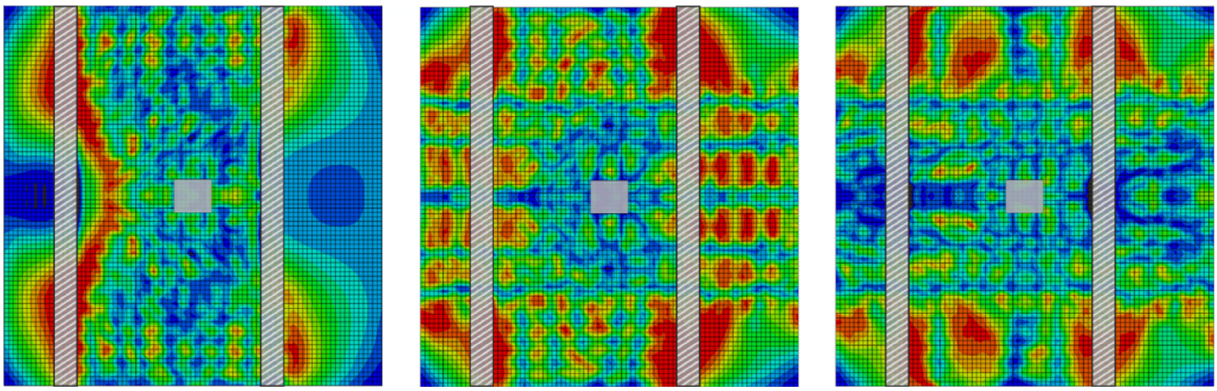

FIGURE 17 Cracking pattern at failure (red: not-cracked; green: tension softening; blue: open crack or compression): (a) $T/T_{cr} = 0$; (b) $T/T_{cr} = 0.7$; (c) $T/T_{cr} = 1.3$

for different values of the effective depth, reinforcement ratio, or concrete compressive strength than those of the specimens tested. This is also the reason why ACI 318 yields more conservative results than EC-2. Both codes add the tensile stresses to the shear strength multiplying σ_t by a similar factor (0.167 for ACI and 0.15 for EC-2), but for the geometry of the tested slabs, the ratio between both codes prediction when $\sigma_t = 0$ *is* $V_{R,EC2}/V_{R,ACI} = 1.37$. Thus, in this case, for the same value of σ_t, the relative reduction of the shear strength is greater for ACI 318.

The results of the experimental campaign presented herein are more or less in line with the observations made in the only similar experiment available in literature, conducted by Regan,[8] when a 15% reduction on the strength was reported for $\sigma_t \approx 3.95$ MPa. This value is greater than the values obtained by the authors, but it is reasonable since the point load was applied at mid-span and a punching-shear failure occurred. Because of that, part of the failure surface was normal to the transverse tensile stresses and the strength of the specimen could have been more affected. However, in the experimental campaign carried out by Bui et al.[8] on slabs subjected to longitudinal tensile stresses, greater relative strength reductions up to a 27% were obtained for values of around 1.2 MPa. This greater values of strength reduction seems to highlight the different degree of affectation between transverse and longitudinal tensile stresses. In any case, the experimental evidence in slabs is scarce and more research is needed in slabs with different geometries, reinforcement ratios, reinforcement dispositions (symmetric or not) and supporting conditions.

To conclude, cracking patterns obtained for different values of the applied external tension are presented in Figure 17, showing a considerable similarity with the experimentally observed crack patterns.

5 | CONCLUSIONS

Based on all the experimental work reported throughout the last decades and on the observations made during the experimental campaign presented in this article, the following conclusions can be drawn:

1. Code formulations are, in general, not clear about how to proceed when predicting the effects of transverse tensile forces on the shear strength of one-way slabs. It is probably due to the fact that they are originally intended for beams, where only longitudinal axial stresses may take place in practice. It is not mentioned if transverse normal stresses should be considered in the same way as longitudinal stresses or even if they may be neglected. The comparison between code

predictions and experimental and numerical results carried out in this study shows that the shear strength is barely affected by the transverse tensile stresses, and neglecting its negative contribution leads only to slightly unsafe results, for the particular case of the specimens tested. On the contrary, if transverse tensile stresses are taken into account, their value should be lessened or very conservative results will be obtained.

2. The decrement in the one-way shear strength due to axial tension can be managed if enough reinforcement is provided to keep crack width under control. Also a uniform or symmetrical distribution of the reinforcement within the concrete cross-section has a favorable effect on the shear strength.
3. For the studied case of one-way slabs subjected to transverse axial tension, no significant reduction of the shear strength has been observed. An approximately linear decrement up to a 5.3% reduction on the shear strength for the highest transverse axial load applied ($\sigma_t \approx 4.2$ MPa) was obtained experimentally. These values are smaller than the relative strength reduction of the shear strength reported in tests on slabs subjected to longitudinal axial tension (27% reduction for $\sigma_t \approx 1.2$ MPa), which highlights the difference in the degree of affectation on the one-way shear strength of transverse and longitudinal tensile stresses.
4. Transverse axial load affects the stiffness of the members due to premature cracking of concrete. If not enough reinforcement is provided in the transverse direction, this fact may lead to a non-fulfillment of the serviceability limit state of deformations and affects the durability of the member due to excessive crack width.
5. The numerical model developed for the non-linear analysis of the tested slabs, calibrated with the experimental results of the tested reference slab ($T = 0$), predicts an approximately linear decrement of the shear strength with increasing axial tension, as observed experimentally, but yields slightly conservative results, particularly for values of $T/T_{cr} > 1.2$. For the aforementioned case of the highest transverse axial load applied at the laboratory ($\sigma_t \approx 4.2$ MPa), the numerical model predicts an 11.8% reduction in the shear strength, compared with the 5.3% reduction observed experimentally.

NOTATIONS

a_v	clear shear span. Distance between the inner face of the support and the inner face of the loading plate
A_c	composite concrete and steel cross-sectional area of the slab
$d_{\max}$	largest nominal maximum aggregate size
d	effective depth of the longitudinal tensile reinforcement
f_c	concrete compressive strength
f_{ck}	characteristic concrete compressive strength
f_{ct}	tensile strength of concrete
f_y	yield stress of the reinforcement
G_f	fracture energy
T	external tensile force
T_{cr}	tensile force associated to the section cracking in pure tension
V_R	shear strength
w	Crack width
ε_{c0}	yielding strain of concrete in compression
ε_{cu}	failure strain of concrete in compression
ν	Poisson's ratio
ρ	reinforcement ratio
σ_t	tensile stresses action on the concrete specimens

ACKNOWLEDGMENTS

This work has been carried out within the framework of the research project BIA-2015-64672-C4-1-R, financed by the Ministry of Economy and Competitiveness (MINECO) of Spain, and with the invaluable help of the technicians and the director of the Laboratory of Technology of Structures and Materials of the Universitat Politècnica de Catalunya. The authors want also to thank Master students Pau Figueras and Laura Beltran who collaborated in the numerical predictions and execution of the tests, respectively.

DATA AVAILABILITY STATEMENT

The data that support the findings of this study are available from the corresponding author upon reasonable request.

ORCID

Pablo G. Fernández https://orcid.org/0000-0002-8237-860X
Antonio Marí https://orcid.org/0000-0002-0994-0715
Eva Oller https://orcid.org/0000-0002-0845-3587

REFERENCES

1. Elstner RC, Richard C, Hognestad E. Laboratory investigation of a rigid frame failure. ACI J Proc. 1957;53(1):637–68.
2. Mattock AH. Diagonal tensional cracking in concrete beams with axial forces. J Struct Div (ASCE). 1969;95(9):1887–900.
3. Haddadin MJ, Hong ST, Mattock AH. Stirrups effectiveness in reinforced concrete beams with axial force. J Struct Div (ASCE). 1971;97(9):2277–97.
4. ACI Committee 318. Building code requirements for reinforced concrete (ACI 318-71). Detroit: American Concrete Institute; 1971. p. 78.
5. Regan PE. Beams subjected to axial loads. London: Imperial College; 1971.p. 93–118.
6. Abrams JH. The punching shear strength of pre-cracked reinforced concrete in biaxial tension. MS Thesis, Cornell University; 1979.

7. Jau WC, White RN, Gergely P. Behavior of reinforced concrete slabs subjected to combined punching and biaxial tension. New York: US Nuclear Regulatory Commission; 1982.
8. Regan PE. Punching shear in prestressed concrete slab bridges. London: Engineering Structures Research Group, Polytechnic of Central London; 1983.
9. Vecchio FJ, Collins MP. Modified compression field theory for reinforced concrete elements subjected to shear. ACI J Proc. 1986;83(2):219–31.
10. Bhide SB, Shrinivas B, Collins MP. Influence of axial tension on the shear capacity of reinforced concrete members. ACI Struct J. 1989;86(5):570–81.
11. Collins MP, Adebar P. Shear strength of members without transverse reinforcement. Can J Civ Eng. 1996;23(1):30–41.
12. Xie L, Bentz EC, Collins MP. Influence of axial stress on shear response of reinforced concrete elements. ACI Struct J. 2011; 108(6):745–54.
13. Jorgensen HB, Hoang LC, Fabrin LS, Malgaard J. Influence of high axial tension on the shear strength of non-shear RC beams. Proc Int IABSE Conf. 2013;99(31):86–93.
14. European Committee for Standardization. Eurocode 2: design of concrete structures: part 1: general rules and rules for buildings. Brussels, Belgium: ECS; 2002.
15. Fernández-Montes D, González E, Díaz E. Influence of axial tension on the shear strength of floor joist without transverse reinforcement. Struct Concr. 2015;16(2):207–20.
16. Bui TT, Nana WSA, Abouri S, Liman A, Tedoldi B, Roure T. Influence of uniaxial tension and compression on shear strength of concrete slabs without shear reinforcement under concentrated loads. Construct Build Mater. 2017;146:86–101.
17. Fernández PG, Marí A, Oller E. Theoretical prediction of the punching shear strength of concrete flat slabs under in-plane tensile forces. Eng Struct. 2021;229(3):1116–32.
18. Deifalla A. A mechanical model for concrete slabs subjected to combined punching shear and in-plane tensile forces. Eng Struct. 2021;231:111787.
19. ACI Committee. ACI Committee 318: Building code requirements for structural concrete and commentary (ACI 318-19). Farmington Hills: American Concrete Institute; 2019.
20. Fernández PG, Marí A, Oller E. Punching-shear strength of reinforced concrete slabs subjected to unidirectional in-plane tensile forces. Struct Concr. 2020;22(2):1223–38.
21. Nana WSA, Bui TT, Liman A, Abouri S. Experimental and numerical modelling of shear behavior of full-scale RC slabs under concentrated loads. Structure. 2017;10:96–116.
22. Reissen K, Hegger J. Shear capacity of reinforced concrete slabs under concentrated loads. Seoul: IABSE Congress Report; 2012.
23. Lantsoght E, van der Veen C, Walraven JC. Shear in one-way slabs under concentrated loads close to support. ACI Struct J. 2013;110(2):275–84.
24. Bui TT, Abouri S, Liman A, Nana WSA, Tedoldi B, Roure T. Experimental investigation of shear strength of full-scale concrete slabs subjected to concentrated loads in nuclear buildings. Eng Struct. 2016;113:405–20.
25. Reissen K, Hegger J. Shear in reinforced concrete slabs – experimental investigations in the effective shear width of one-way slab under concentrated loads and different degrees of rotational restraint. Struct Concr. 2018;19:36–48.
26. Havolnik J, Vidakovic A, Vida R. Shear capacity of clamped deck slabs subjected to a concentrated load. J Bridge Eng. 2020; 25(7):794–802.
27. Lantsoght E, van der Veen C, Walraven JC. Shear capacity of slabs under a combination of loads. Israel: Fib Symposium; 2013.
28. Dassault Systems Simulia Corp. Abaqus analysis user's manual 6.14. Providence, RI: Dassault Systèmes Simulia Corp; 2014.
29. Lubliner J, Oliver J, Oller S, Oñate E. A plastic-damage model for concrete. Int J Solids Struct. 1988;25(3):299–326.
30. Lee J, Fenves GL. Plastic-damage model for cycling loading of concrete structures. J Eng Mech. 1998;124(8):892–900.
31. Fédération Internationale du Béton (FIB). Fib model code for concrete structures 2010. Lausanne, Switerland: FIB; 2013.
32. Cladera A, Marí A, Bairán JM, Oller E, Duarte N. The compression chord capacity model for the shear design and assessment of reinforced and prestressed concrete beams. Struct Concr. 2016;18(2):1017–32.

AUTHOR BIOGRAPHIES

Pablo G. Fernández,
Universitat Politècnica de Catalunya, Department of Civil and Environmental Engineering,
Campus Nord Jordi Girona 1-3, C-1 201, 08034 Barcelona, Spain
pablo.gonzalo.fernandez@upc.edu

Antonio Marí,
Universitat Politècnica de Catalunya, Department of Civil and Environmental Engineering,
Campus Nord Jordi Girona 1-3, C-1 201, 08034 Barcelona, Spain
antonio.mari@upc.edu

Eva Oller
Universitat Politècnica de Catalunya, Department of Civil and Environmental Engineering,
Campus Nord Jordi Girona 1-3, C-1 201, 08034 Barcelona, Spain
eva.oller@upc.edu

How to cite this article: Fernández PG, Marí A, Oller E. Experimental investigation of the shear strength of one-way reinforced concrete (RC) slabs subjected to concentrated loads and in-plane transverse axial tension. Structural Concrete. 2021; 22:3661–76. https://doi.org/10.1002/suco.202100447